A R C H I V E S O F M E T A L L U R G Y A N D M A T E R I A L S
Volume 60 2015 Issue 4
DOI: 10.1515/amm-2015-0273

P. KULA*, W. SZYMAŃSKI, Ł. KOŁODZIEJCZYK*,#, R. ATRASZKIEWICZ*, K. DYBOWSKI*, J. GRABARCZYK*, R. PIETRASIK*, P. NIEDZIELSKI*, Ł. KACZMAREK*, M. CŁAPA*

HIGH STRENGTH METALLURGICAL GRAPHENE – MECHANISMS OF GROWTH AND PROPERTIES

GRAFEN METALURGICZNY O WYSOKIEJ WYTRZYMAŁOŚCI – MECHANIZMY WZROSTU I WŁAŚCIWOŚCI

In this work, the growth mechanisms of chemical vapor deposited and metallurgical graphene and their selected mechanical and electrical properties were investigated. The study revealed the influence of the growth mechanisms on mono- and poly-crystalline nanostructures of synthesized graphene monolayers. The structure of flake boundaries greatly affects both the mechanical and electrical properties. The key factors are overlapping of the graphene flakes, their degree of mismatch and the presence of π type bonds. All of these issues should be taken into account when developing industrially scaled technologies for graphene manufacturing.

Keywords: graphene; growth mechanism; electrical properties

W pracy przedstawiono wyniki badań mechanizmów wzrostu oraz wybranych właściwości mechanicznych i elektrycznych grafenu chemicznie osadzanego z fazy gazowej oraz grafenu metalurgicznego. Badania wykazały wpływ mechanizmów wzrostu na mono- i polikrystaliczne nanostruktury syntetyzowanych monowarstw grafenu. Struktura granic płatków grafenu znacząco wpływa zarówno na właściwości mechaniczne jak i elektryczne. Kluczowymi czynnikami są: nakładanie się płatków grafenu, stopień ich niedopasowania oraz obecność wiązań typu π. Wszystkie te aspekty powinny być brane pod uwagę przy opracowywaniu technologii produkcji grafenu na skalę przemysłową.

1. Introduction

Perfect graphene has extremely high strength ~ 130 GPa and a modulus of ~ 1 TPa [1,2]. These properties make graphene a material with potential for use in the polymer industry, such as in future graphene-reinforced composites. Measurable and satisfactory strengthening effects can be achieved by encapsulating graphene sheets (up to two layers) between layers of the polymer [1]. For graphene electronic applications, it is important to establish a relationship between the electrical properties and the material stress state. By altering the stress, the mobility of the electric charge can be changed, which is particularly important for applications in electronic circuits such as field-effect transistors, transparent electrodes on flexible substrates and strain gauges [3,4]. Most of the studies on the impact of the graphene deformation on its properties are model-based research using molecular dynamics [5–7]. Often, this type of research does not consider defects in the graphene structure and impurities that occur on the surface as a result of the processes associated with the formation of graphene-based systems. The transfer of graphene using polymethylmethacrylate (PMMA) is one such process. Despite being the most popular transfer method, it has disadvantages, one of them being remaining residual PMMA after the transfer process [8]. These residues have a significant effect on the electrical properties [8–10]. In this case, modeling does not replace experiments conducted on real structures. The most commonly used graphene sheets are obtained by exfoliation from highly oriented pyrolytic graphite (HOPG) [11] or by a chemical vapor deposition (CVD) process on transistor circuits or small sensors [12]. In the literature, there is a lack of a broad characterization of graphene obtained using other methods. There is only a single reference on the synthesis of graphene from the liquid phase [13]. Moreover, there are no studies on the large area manufacturing of graphene. Efficient new functional applications for graphene require industrially scaled manufacturing methods.

The most common CVD graphene is a polycrystalline 2-dimensional material composed of partially overlapped, randomly oriented flakes [4]. This type of structure results from the spontaneous and random nucleation of graphene flakes onto a solid body that is not perfectly flat [14]. The disorientation and overlapping causes the CVD graphene properties to be significantly different than the theoretical properties and those for exfoliated graphene [15]. Recently, alternative industrial methods for graphene sheets manufacturing have been developed. They are based on the controlled carbon precipitation from liquid metallic matrices

* LODZ UNIVERSITY OF TECHNOLOGY, INSTITUTE OF MATERIALS SCIENCE AND ENGINEERING, 1/15 STEFANOWSKIEGO STR., 90-924 LODZ, POLAND
# Corresponding author: lukasz.kolodziejczyk@p.lodz.pl

[16,17]. Such manufactured graphene sheets have exhibited extremely high mechanical strength and are known as High Strength Metallurgical Graphene (HSMG)*.

The work presents a structural investigation to determine the HSMG growth mechanism, as well as a functional characterization of the HSMG. The results of the static tensile tests, basic electrical properties as well as the gas sorption abilities are presented for HSMG and are compared to CVD graphene.

2. Material and methods

The HSMG sheets were synthesized in an industrially scaled thermochemical facility based on the process described in [16,17]. Different hydrocarbon gas flows as well as heating/cooling conditions were applied to determine both the stages and growth mechanisms for the HSMG. Prior to the mechanical and electrical property investigations, all of the samples were subjected to structural analysis. The graphene quality was studied using Raman spectroscopy (inVia Renishaw). A JEOL JSM-6610LV scanning electron microscope (SEM) integrated with MiniCL-GATAN Cathodoluminescence Imaging and Oxford Instruments systems was used for imaging the graphene samples. Electron diffraction analysis was performed on a Philips EM300 transmission electron microscopy (TEM). Thereafter, continuous mono-/bilayers of HSMG were synthesized and then transferred onto different substrates to prepare the samples for property measurements. The transfer procedure for the HSMG and commercially available CVD graphene sheets (Graphene Supermarket, USA) was based on the modified method of graphene transfer from metallic substrates on thin PMMA films, which is fully described in our previous paper [16]. Similar methods and their variations are most often utilized in procedures for graphene transfer on any substrate. Substrate materials of polyethylene, polyimide and glass were used.

Static tensile tests of the conductive and semiconducting HSMG (abbreviated as c-HSMG and sc-HSMG, respectively) and CVD graphene sheets supported on a 200 µm thick low-density polyethylene (LDPE) substrate were carried out using a CETR UMT-2 universal test system (Bruker Corporation, USA) equipped with positioning system with a resolution of 0.5 µm and a 2-axis load sensor (0.2-25 N) with a resolution of 1 mN. The size of the LDPE substrate was 20 x 15 mm, whereas the size of the transferred graphene sheets was 12 x 6 mm. Simultaneously, the graphene sheet resistance was measured during each test. The tensile test setup is shown in Fig. 1a. The failure mechanisms for the graphene were observed in all specimens after tensile testing using SEM imaging. The testing equipment for measuring the resistance vs. temperature behavior of the graphene samples consisted of a vacuum chamber equipped with a vacuum pump and gas flow system. The graphene samples were placed on the measurement table that was heated and chilled using a Peltier's module system (Fig. 1b).

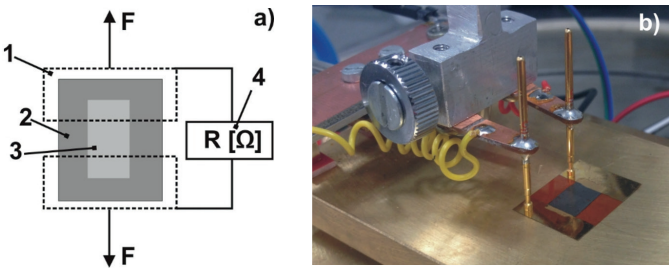

Fig. 1. a) The tensile test setup with continuous resistance monitoring: 1-clamps, 2-supporting substrate, 3-graphene and 4-multimeter, b) portion of the measurement setup (inside the vacuum chamber) for resistance vs. temperature characterization of the graphene.

The testing stand enabled control over the atmosphere as well as the temperature and permitted resistance monitoring. The graphene sheets (12 x 6 mm) were then transferred onto 25 µm thick polyimide with dimensions of 20 x 15 mm (Advent Research Materials, Oxford, UK) or glass cover-slip substrates. Then, gold connectors were deposited to obtain a measurement area of 6 x 6 mm. The resistance of the graphene sheets was measured cyclically at temperature intervals from 253K to 333K (-20÷60°C). The measurement of the electrical properties was conducted under 1 Pa vacuum conditions.

3. Results and discussion

3.1. Electrical properties measurement

Results of the resistance measurements vs. temperature (Fig. 2) revealed an essential difference between the two types of HSMG graphene, namely those grown using the dendritic mode and formed using the cellular mode.

The first exhibited a positive temperature coefficient of resistance, which is typical for electrical conductors (Fig. 2b) and is similar to CVD graphene (Fig. 2a). Therefore, this type of graphene was abbreviated as c-HSMG. The second type behaved like a semiconductor, with a negative temperature coefficient of resistance (Fig. 2c), and is thus abbreviated as sc-HSMG. Moreover, the sorption and desorption effects are clearly observed (marked by arrows). The calculated values of the temperature coefficients of resistance of c-HSMG, sc-HSMG and CVD graphene are gathered in the Table 1.

TABLE 1
The experimental results for the temperature coefficients of resistance

	Temperature coefficient of resistance [1/K]
sc-HSMG	$-1.7\cdot10^{-3} \div -4.0\cdot10^{-4}$
c-HSMG	$3.5\cdot10^{-4} \div 4.1\cdot10^{-4}$
CVD graphene	$1.5\cdot10^{-4} \div 4.0\cdot10^{-4}$
exfoliated graphene monolayer*	$-1.5\cdot10^{-3}$
reduced graphene oxide monolayer [18]	$-9.5\cdot10^{-4}$

* calculated from [15]

* KULA P, PIETRASIK R, KAZIMIERSKI D, ATRASZKIEWICZ R, DYBOWSKI K, SZYMANSKI W, ET AL. RESISTANCE-TEMPERATURE CHARACTERISTICS OF CVD AND HIGH STRENGTH METALLURGICAL GRAPHENE (HSMG), INT. J. NANOTECHNOLOGY (SUBMITTED)

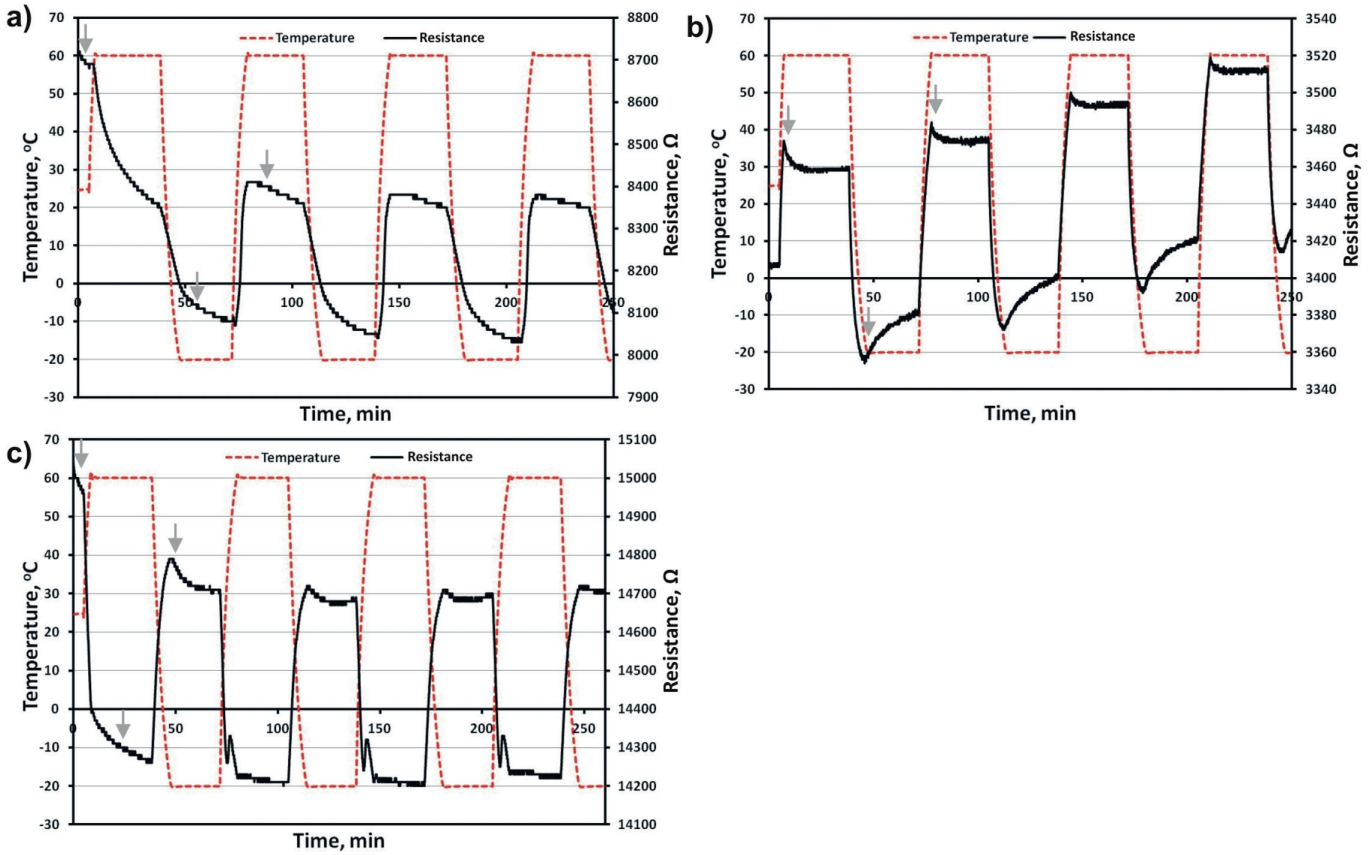

Fig. 2. Evolution of the temperature and resistance changes as a function of time: a) CVD, b) c-HSMG graphene (in-phase relationship) and c) sc-HSMG graphene (anti-phase relationship)

The experimental results are consistent with the data published in the literature [15,18]. For both the exfoliated graphene and the reduced graphene oxide, the coefficient of resistance is comparable with the values obtained for the sc-HSMG.

These results also indicate the importance of a flake's grains structure in determining the electrical conductivity of industrially scaled graphene (which is discussed in the next section). Both, the significant contribution of the π-type bonds in the overlapping zone for CVD graphene and their local appearance for c-HSMG likely reshaped the band structure of the electrical conductivity. However, the lack of π-type bonds in the perfect hexagonal structure of the sc-HSMG contributed to it retaining its semiconductor behavior.

3.2. Mechanisms of graphene growth

The results of the nanostructural investigations of the graphene quality are presented in Fig. 3. All of the types of investigated graphene exhibited very similar Raman spectra. This confirmed the presence of single/bilayer graphene with a typical ratio of intensity and a full width at half maximum (FWHM) of the selected Raman peaks (Table 2) [19,20].

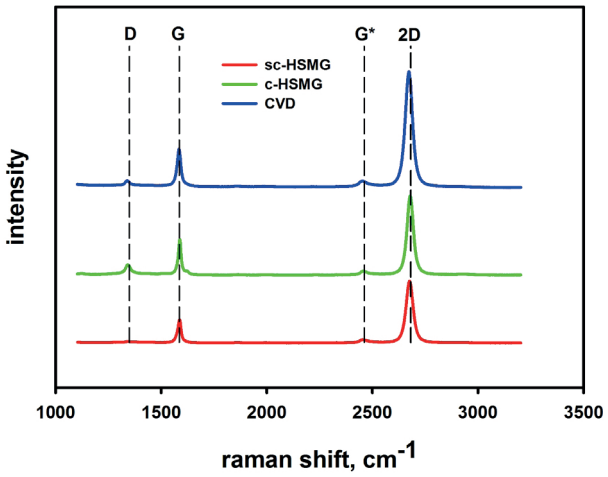

Fig. 3. Raman spectra of all studied graphene samples

TABLE 2
Ratios of the typical peaks and FWHM calculated from the Raman spectra deconvolution

	CVD	c-HSMG	sc-HSMG
I_G/I_{2D}	0.313	0.435	0.364
2D - FWHM [cm^{-1}]	41.028	34.712	38.643

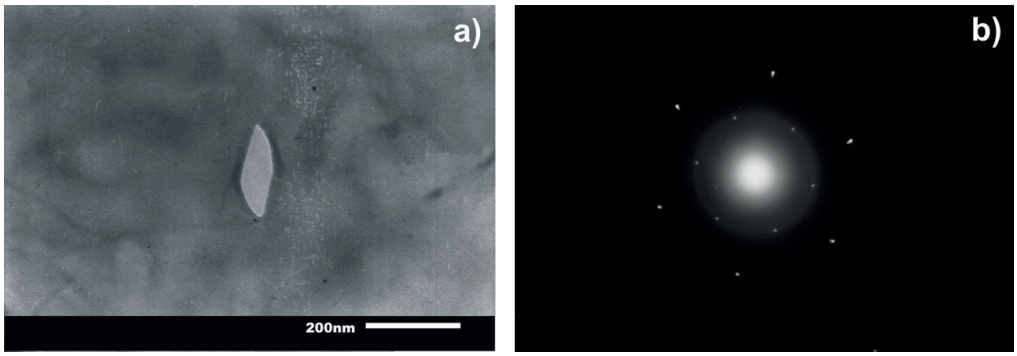

Fig. 4. a) SEM image of the HSMG supported partially on a TEM mesh grid (square mesh ~40 μm, fine mesh diameter ~2 μm) and b) TEM electron diffraction pattern of the HSMG

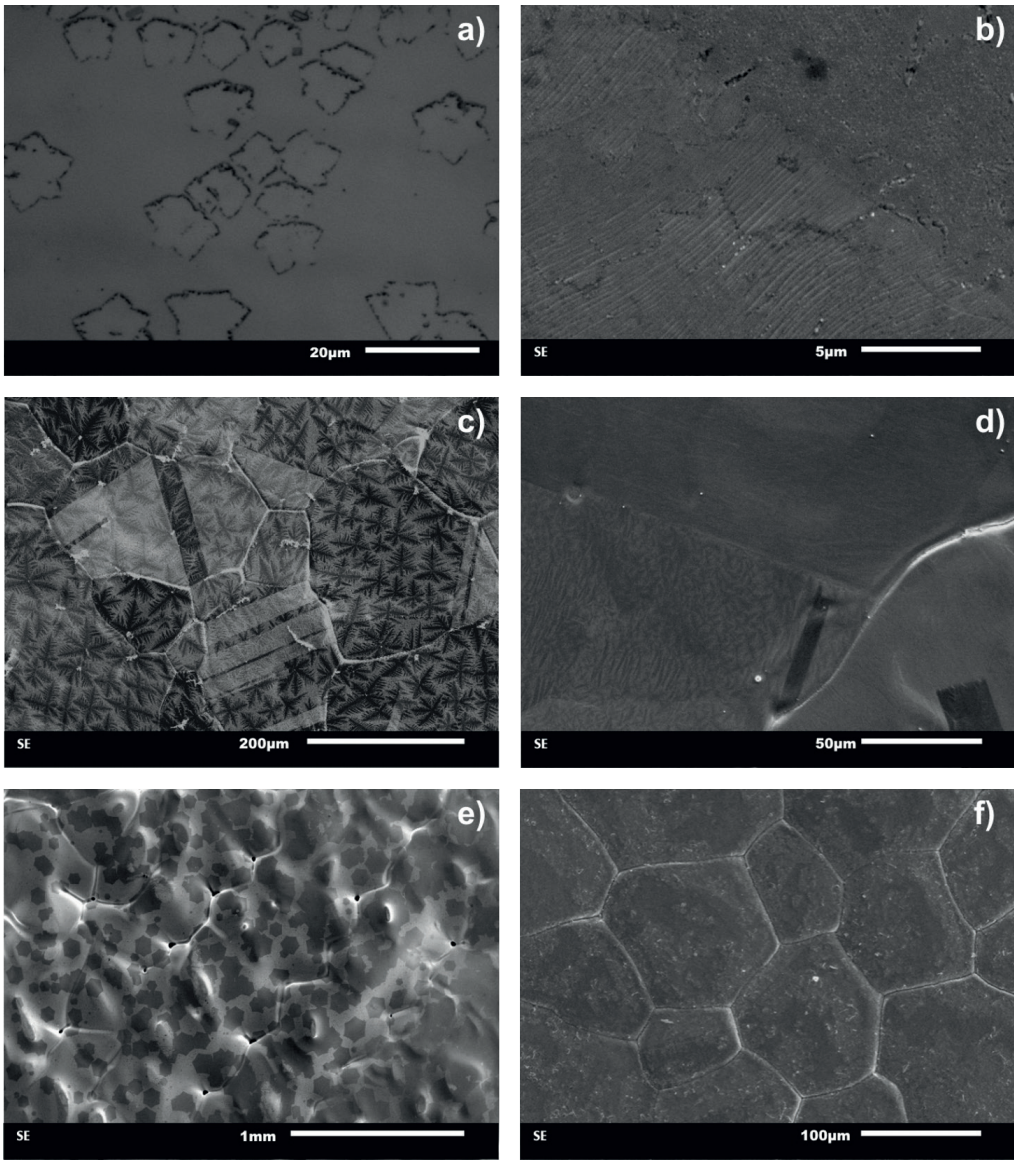

Fig. 5. Mechanisms for graphene growth: a) and b) random distribution and wrinkles on CVD graphene flakes, c) and d) dendritic growth of the c-HSMG grapheme and e) and f) cellular growth of the sc-HSMG graphene. All images are from the SEM with the exception of a), which was acquired on an optical microscope

Based on the SEM and TEM analyses (Fig. 4), three different mechanisms for graphene growth were revealed.

The CVD graphene nucleates from a gaseous phase on solid copper randomly (Fig. 5). The star-like graphene nuclei

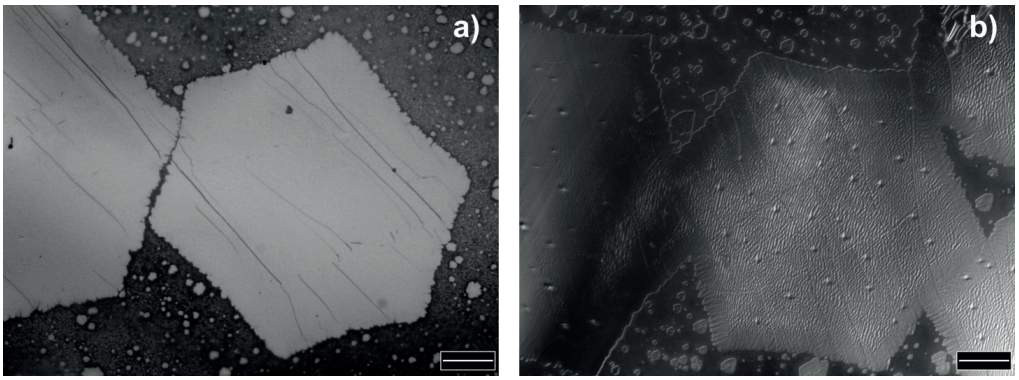

Fig. 6. Nucleation of hexagonal graphene on a liquid metallic matrix: a) before arrangement of two graphene hexagons and b) perfect hexagonal atomic arrangement between neighboring graphene flakes. The scale bars measure 20 μm

continue growing until fully covering the solid matrix.

A slight overlapping of neighboring graphene flakes occurs, providing continuity in the graphene sheet [4]. That is why the CVD graphene grains boundaries are likely bilayered and held together by π-bonds. That small contribution of the π-bonds may exert considerable influence on the band structure of the CVD grapheme, as well as its mechanical properties. The CVD graphene sheet on the copper matrix is weakly adhered to the substrate. The differing thermal expansion coefficient between the copper and graphene causes visible wrinkling in the CVD graphene during cooling after deposition. However, the CVD graphene is strong enough to resist intensive bending when the copper substrate is deformed by twinning (Fig. 5a, b). The graphene sheets formed on liquid metal revealed two different mechanisms for nucleation and growth. In the first one mechanism, the growth starts according to the dendritic 2D mode (Fig. 5c and 5d).

The growth of numerous nuclei proceeds very fast in certain crystal directions. The longest branches contact, stabilizing their random orientations. If the growth rate of the dendrite branches is fast enough, they can locally overlap even if they crystallize on an absolutely flat liquid metal surface due to crystallographic disorientation. Consequently, the metallurgical graphene grown in this way is also a polycrystalline single layer material. The grains (flakes) exhibit a random orientation and few π-bonds exist in overlapping sites.

The alternative mechanism for forming graphene on liquid metal is based on cellular (hexagonal) nucleation and growth (Fig. 5e and 5f). All of the nuclei exhibit a hexagonal shape and are able to move with three degrees of freedom on the surface of the liquid metal (including rotation). Therefore, conformable accommodation along hexagon edges occurs when they contact (Fig. 6a). In this way, perfect hexagonal atoms arrangement can continue between neighboring flakes (Fig. 6b) and consequently, large monolayer areas of semi perfect graphene may be formed without any π-bonds.

3.3. Tensile tests

The resistance vs. displacement plots, which were measured during tensile testing, are presented in Fig. 7.

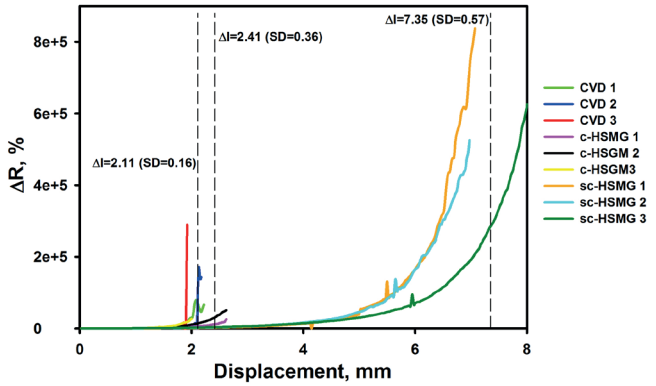

Fig. 7. Evolution of the electrical resistance during tensile testing of the examined graphene samples

There were fundamental differences found between the mechanical and electrical behavior of the graphene samples grown via different crystallization mechanisms. The plot above shows that the CVD graphene loses electrical contact within the shortest time for all of the graphene samples tested. The loss of electrical contact occurs at a relative elongation of ε = 52.7% (Δl = 2.11±0.16 mm). The nature of the electrical contact loss is sudden, which results in a very rapid jump in the resistance. The measured average initial electrical resistance for the CVD graphene samples was RCVD = 56.4±22.2 kΩ. Shortly before loss of contact, the maximum resistance was approximately 1500 times greater than the initial resistance. A significantly different evolution was observed for the resistance curves of the graphene samples grown from a liquid forming matrix. In this case, the electric resistance increases smoothly with the displacement and the loss of contact occurs without a sudden increase in the resistance. It is noted that the tensile test of the c-HSMG graphene started at a much higher average initial resistance $R_{c\text{-}HSMG}$ = 181.9±55.5 kΩ. In contrast, the relative elongation at which electrical contact was lost was ε = 60.25% (Δl = 2.41±0.36 mm), which is 7.55% higher than the CVD graphene. The maximum measured resistance was ~500 times higher than the initial value. Surprisingly, high values of relative elongation were observed for the graphene formed on the liquid matrix using the cellular growth method, ε = 183.75% (Δl = 7.35±0.57 mm). In the case of the sc-HSMG graphene, the lowest initial resistance was $R_{sc\text{-}HSMG}$ = 8.0±1.5 kΩ and the resistance at the maximum elongation increased ~5000 times compared with the initial value.

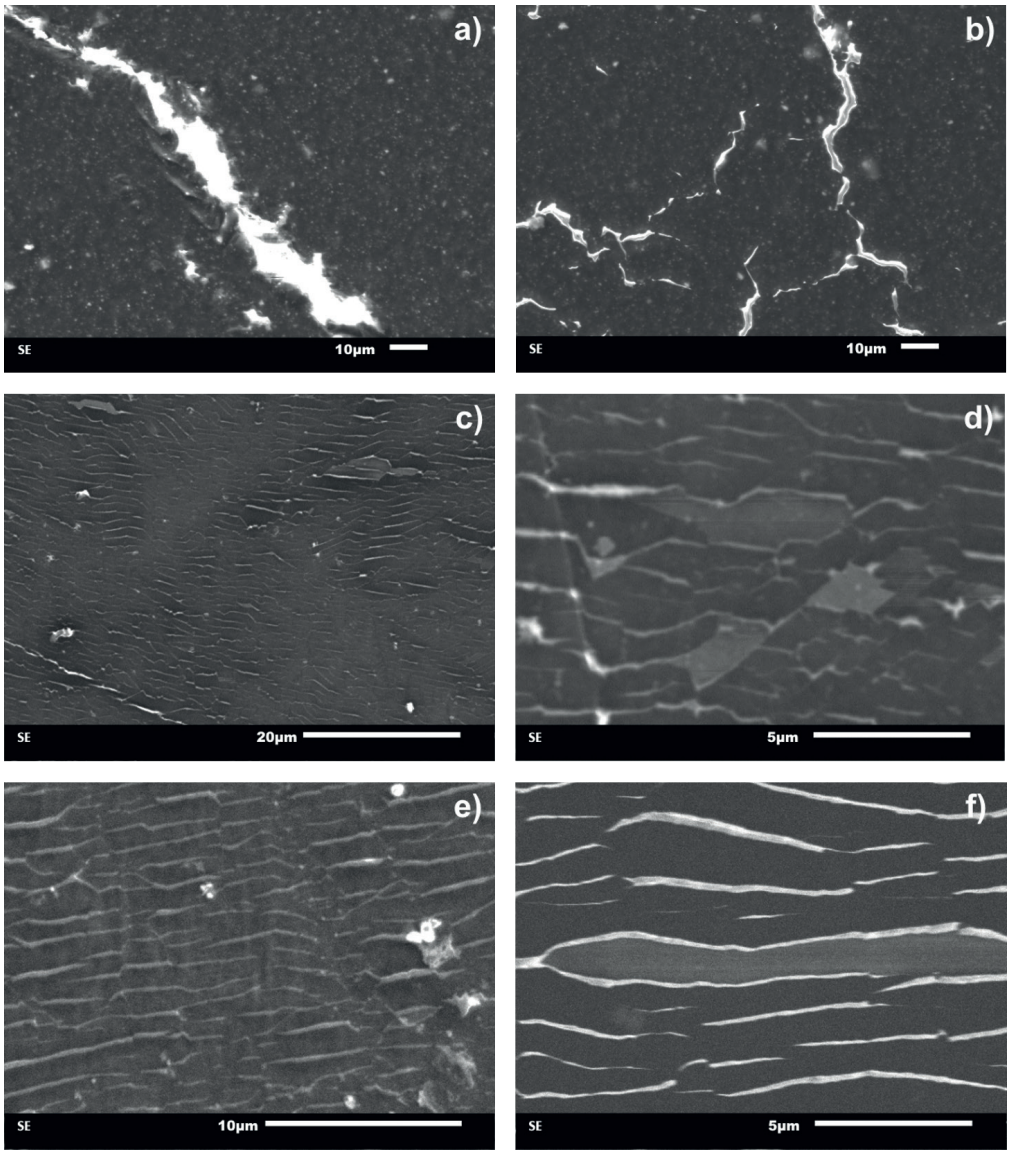

Fig. 8. SEM images of graphene supported on an LDPE substrate after tensile testing: a and b) CVD graphene with undirected cracks (not perpendicular to the direction of applied tensile force), c and d) c-HSGM graphene with cracks running perpendicular and angled at 60° to the direction of applied force and e and f) sc-HSGM graphene with cracks running perpendicular to the direction of applied force

The SEM observations of the graphene samples after tensile testing revealed the failure mechanisms. The CVD graphene fractured primarily along the flake boundaries (Fig. 8a). A dominant arrangement of cracks was observed at an angle of 45° with respect to the direction of the applied tensile force (Fig. 8b). These observations reveal the weakness of CVD graphene flakes boundaries and the presence of slip plane in the maximum shear stress direction. Such a failure mechanism for CVD graphene may result from an overlapping of flakes at the boundaries and the existence of weak π-type bonds at these locations. Both the HSMG graphene samples, grown in the dendritic and cellular modes, fractured perpendicular to the direction of the applied tensile force, exclusively (Fig. 8c-f). Only several cracks angled at 60 degrees revealed the existence of locally defective grains in the c-HSMG (Fig. 8d). Such a failure is the result of the continuity of the perfect hexagonal atomic arrangement on the macro scale and/or from the high strength of the coplanar low angle grain boundaries. Thus, the suggested overlapping of the fast growing dendrites acts locally without any visible influence on the high strength or the failure mechanism of the HSMG.

The three types of industrially scaled single/bilayer graphene investigated here reveal different mechanical strength and electrical properties, despite exhibiting very similar Raman spectra and TEM electron diffraction patterns. The comparative data about their growth mechanisms as well as their mechanical and electrical behavior are collected in Table 3.

The results obtained and summarized in Table 3 confirm that the growth mechanisms of industrially scaled graphene sheets influence their substructure. Particularly, the flake boundary structures have a strong influence on the mechanical and electrical properties. The key factors are likely the overlapping of flakes, their disorientation and the presence of π-type bonds.

TABLE 3

Summary of the properties of the studied graphene samples

	CVD graphene	c-HSMG	sc-HSMG
Forming Cu matrix	solid	liquid	liquid
Growth mechanism	heteroepitaxy	dendritic	cellular
2D microstructure	polycrystalline	polycrystalline	mostly monocrystalline
Grains structure	overlaps	coplanar, low angle	not revealed
Failure mechanism	slip, intercrystalline decohesion	transcrystalline decohesion	transcrystalline decohesion
π type bonds	exist in overlapped zones	exist locally	do not exist
Strain at the loss of conductivity ε [%]	52.7	60.25	183.75
Temperature coefficient of resistance [1/K]	$1.5 \cdot 10^{-4} \div 4.0 \cdot 10^{-4}$	$3.5 \cdot 10^{-4} \div 4.1 \cdot 10^{-4}$	$-1.7 \cdot 10^{-3} \div -4.0 \cdot 10^{-4}$
Type of the band structure	conductor	conductor	semi-conductor

4. Conclusions

In this study, we show that depending on the growth mechanism, using graphene synthesized from a liquid phase permits researchers to obtain materials with improved mechanical and electrical properties compared with commonly used CVD graphene. The reason for such an increase in these properties is an important difference in the morphology of grain boundaries. The sc-HSMG exhibited an electrical behavior very close to the theoretical value. Moreover, the tensile test confirmed the substantially higher mechanical strength of sc-HSMG (more than three times higher strain at the conductivity loss) compared with CVD and c-HSMG. Therefore, sc-HSMG sheets seem to be a good candidate for further investigations as a functional nanomaterial for future efficient hydrogen storage systems [21], reinforcing sheets in composites [22], strain sensors [4], filtering membranes [23] and many others.

Acknowledgments

The study is financed by The National Center for Research and Development as part of the GRAF-TECH program, (GraphRoll) entitled: "Graphene nanocomposite for the reversible hydrogen storage", agreement number GRAF-TECH/NCBR/07/24/2013.

REFERENCES

[1] L. Gong, R.J. Young, I.A. Kinloch, I. Riaz, R. Jalil, K.S. Novoselov, ACS Nano **6**, 2086 (2012).
[2] I.A. Ovid'ko, Rev. Adv. Mater. Sci. **34**, 19 (2013).
[3] M.A. Bissett, M. Tsuji, H. Ago, Phys. Chem. Chem. Phys. **16**, 11124 (2014).
[4] X. Li, R. Zhang, W. Yu, K. Wang, J. Wei, D. Wu, A. Cao, Z. Li, Y. Cheng, Q. Zheng, R.S. Ruoff, H. Zhu, Sci. Rep. **2**, 870 (2012).
[5] S.-M. Choi, S.-H. Jhi, Y.-W. Son, Nano Lett. **10**, 3486 (2010).
[6] K.I. Tserpes, Acta Mech. **223**, 669 (2011).
[7] A. Hadizadeh Kheirkhah, E. Saeivar Iranizad, M. Raeisi, A. Rajabpour, Solid State Commun. **177**, 98 (2014).
[8] Y.-C. Lin, C.-C. Lu, C.-H. Yeh, C. Jin, K. Suenaga, P.-W. Chiu, Nano Lett. **12**, 414 (2012).
[9] H. Park, P.R. Brown, V. Bulović, J. Kong, Nano Lett. **12**, 133 (2012).
[10] A. Pirkle, J. Chan, A. Venugopal, D. Hinojos, C.W. Magnuson, S. McDonnell, L. Colombo, E.M. Vogel, R.S. Ruoff, R.M. Wallace, Appl. Phys. Lett. **99**, 122108 (2011).
[11] H. Shioya, M.F. Craciun, S. Russo, M. Yamamoto, S. Tarucha, Nano Lett. **14**, 1158 (2014).
[12] S.-K. Lee, B.J. Kim, H. Jang, S.C. Yoon, C. Lee, B.H. Hong, J.A. Rogers, J.H. Cho, J.-H. Ahn, Nano Lett. **11**, 4642 (2011).
[13] D. Geng, B. Wu, Y. Guo, L. Huang, Y. Xue, J. Chen, G. Yu, L. Jiang, W. Hu, Y. Liu, Proc. Natl. Acad. Sci. U. S. A. **109**, 7992 (2012).
[14] L.P. Biró, P. Lambin, New J. Phys. **15**, 035024 (2013).
[15] Q. Shao, G. Liu, D. Teweldebrhan, A.A. Balandin, Appl. Phys. Lett. **92**, 202108 (2008).
[16] L. Kolodziejczyk, P. Kula, W. Szymanski, R. Atraszkiewicz, K. Dybowski, R. Pietrasik, Tribol. Int. (2014), DOI: 10.1016/j.triboint.2014.12.003 (in press).
[17] P. Kula, R. Pietrasik, K. Dybowski, R. Atraszkiewicz, W. Szymanski, L. Kolodziejczyk, P. Niedzielski, D. Nowak, Appl. Mech. Mater. **510**, 8 (2014).
[18] K.S. Vasu, B. Chakraborty, S. Sampath, A.K. Sood, Solid State Commun. **150**, 1295 (2010).
[19] A. Das, B. Chakraborty, A.K. Sood, Bull. Mater. Sci. **31**, 579 (2007).
[20] A.C. Ferrari, J.C. Meyer, V. Scardaci, C. Casiraghi, M. Lazzeri, F. Mauri, S. Piscanec, D. Jiang, K.S. Novoselov, S. Roth, A.K. Geim, Phys. Rev. Lett. **97**, 187401 (2006).
[21] P. Kula, Ł. Kaczmarek, P. Zawadzki, Ł. Kołodziejczyk, W. Szymański, P. Niedzielski, R. Pietrasik, K. Dybowski, D. Kazimierski, D. Nowak, Int. J. Hydrogen Energy **39**, 19662 (2014).
[22] A. Bhattacharyya, S. Chen, M. Zhu, Express Polym. Lett. **8**, 74 (2014).
[23] Y. Han, Z. Xu, C. Gao, Adv. Funct. Mater. **23**, 3693 (2013).

Received: 20 January 2015.